Egypt. J. Chem. **Vol. 66,** No. **SI 13, 781-795** (2023)

Egyptian Journal of Chemistry

http://ejchem.journals.ekb.eg/

Effect Of Vacuum UV Irradiation And PVA Grafting On Thin-Film Composite RO Membranes

Marwa S.Shalaby[a*], Heba Abdallah[a], Ralph Wilken[b], Schmüser Christoph[b], Ahmed M.Shaban[c], Rania Ramadan [a], Gawel Sołowski[*d]

[a] *Chemical Engineering Department, Engineering Research &Renewable Energy Institute, National Research Centre, Egypt*

[b] *Fraunhofer Institute for Manufacturing Technologies and Advanced Materials (IFAM), Plasma technology and surface treatment, Bremen, Germany,*

[4]*Fraunhofer Institute for Manufacturing Technologies and Advanced Materials (IFAM), Plasma technology and surface treatment, Bremen, Germany,*

[c] *Water Pollution Research Department, Environmental Research Institute, National Research Centre, Egypt,*

[d] *Department of Molecular Biology and Genetics, Faculty of Science and Art, Bingol University, Bingol, 1200, Türkiye*

Abstract

The surface modifications of thin-film composite (TFC) reverse osmosis membranes were investigated in this study. The development led to simplified technology to produce desalinated water. Another research aim was a comparison of change membrane performances by the presence of zinc nanostructures during the deposition of a PVA/GA chemical layer and by surface activation by vacuum UV (VUV) irradiation. Zn -nanostructures and vacuum irradiation strongly influenced salt rejection, chlorine resistance, and antifouling behavior. VUV-irradiation decreased water contact angle on commercial TFC membranes. VUV treatment with a web speed of 1 m/min extended water contact angle on membranes to reach 8.7°. Those results proved the activation effect of VUV-irradiation on the reverse osmosis membrane and increased hydrophilicity. A decrease in VUV dosage led to an increase in web speed and lowered radiation effect. Zn-nanostructures in the PVA coating layer enhanced the fouling resistance and decreased the contact angle by about 10°, obtaining a flux recovery ratio of about 89%. Vacuum UV irradiation showed a significant impact on RO membrane surface modification. Especially for VUV treatment with a web speed of 10 m/min, it showed dense layer deposition, which increased salt rejection to reach 87% but decreased the membrane productivity..

Keywords: Commercial polyamide membranes Chlorine resistance antifouling vacuum UV irradiation Desalination

1. Introduction

Water cleaning, including desalination, is approached by reverse osmosis, a common separation method. The technique uses a membrane in which the relevant part is a selective layer that responds to its efficiency and separated solutions. Selective layers of reverse osmosis (RO) membranes are manufactured from polyamides[1], piperazine[2], cellulose acetate[3] or diacetate[4], and triacetate[5], etc. From the 1960s commercial reverse osmosis membranes used efficiently, for water desalination were based on selective polyamide layers[6]. This membrane is known as a thin-film composite (TFC) membrane. Polyamide is a macromolecule that contains repeating amide groups (-CO-NH-). In TFC membranes, deposited polyamide llayerswere found on the base membrane material with a branched structure caused by applying m-phenylenediamine, and trimesoyl chloride[7]. These polyamide-based TFC RO membranes are determined as capable to reject different solutes at high water throughput[8]. The structure of the surface and so materials used are doped to decrease fouling behavior of TFC RO membranes[9]. In tropical zone countries such as Egypt or Nigeria[10], some special conditions promote the fouling of RO membranes [11], e.g. high salinity, high urban terrains (Cairo) [12], medium temperature proper for bacteria development [13],

*Corresponding author e-mail: marwashalaby14@gmail.com.; (Marwa Saied Shalaby).
Receive Date: 20 January 2023, Revise Date: 06 May 2023, Accept Date: 08 May 2023
DOI: 10.21608/EJCHEM.2023.188560.7484

humic substances[14], and colloids [15]. The presence of disinfecting agents as chlorine or chemicals formed from it causing further limited lifetime for membranes [16]. Chlorination of membrane is commonly performed by chloramine, chlorine dioxide, or hypochlorite salt [17]. Chlorine or other halogens causes a strong oxidative effect, leading to a gradual degradation of the TFC layer, especially in acidic conditions [18]. These effects shorten the lifetime of the RO membrane modules and increase replacement costs. Reverse osmosis, especially with thin layers is efficient, a method to desalinate in quite an economic manner [19,20] in comparison to other membrane systems. This design can easily operate with other systems like dielectric discharge reactors removing of organic compounds especially volatiles in wastewater treatment plants [21]. Therefore, providing RO membranes with antifouling properties while maintaining chlorine resistance is a tool to increase membrane durability and reduce replacement costs [22]. Obstacles found due to limitations in performance and the processes of post treatment processes are adamantly scienced [23,24]. Some research by surface modification improved the hydrophilicity of the TFC [25], expanded fouling resistance [26], and increased salt rejection and chlorine tolerance [27].

In general, increasing the hydrophilicity of membranes grows consecutively with improved flux and selectivity. A large number of membrane surface modifications were tried to improve the antifouling effect [28,29]. PVA is one of the layered materials that can be deposited by simple film deposition from an aqueous solution [30]. Due to the water solubility of the PVA, the PVA is chemically crosslinked with glutaraldehyde (GA) to form acetal bridges [31]. At the same time, crosslinking improved the adhesion between PVA and TFC through covalent bonds. Some researchers have applied PVA as it is a surface modifier to improve hydrophilicity [32] to open new separation applications in different sectors [33]. A challenge was planned to simultaneously enhance both stability with chlorine exposure and anti-fouling behavior of polyamide RO membrane(TFC) [34].

It was known that vacuum UV irradiation of polymers affected beside membrane surfaces but also the outermost micrometers of a substrate [35–37]. Radicals are formed on the surface of polymers during irradiation, along with a generation of excited oxides in an oxygen-containing atmosphere [38]. Therefore functional groups containing oxygen are formed on the surface of polymeric membrane, which improved wettability and increased surface energy [39].

In this work, PVA will be applied as a coating for RO membranes and crosslinked with glutaraldehyde to improve its surface properties. The effect of PVA when doped with zinc oxide (ZnO) - Glycerolate composite nanoparticles will be studied and compared with previously published work [40]. ZnO nanosolution entrapped in PVA layer was studied to present its effect on fouling behavior and chlorine exposure for commercial RO membranes. In addition, the effect of vacuum UV for surface modification as physical irradiation and membranes performance evaluation in terms of permeation and rejection were presented and compared with pristine commercial RO membranes.

2. Experimental

2.1. Materials

CARL ROTH GmbH- GERMANY kindly supplied us with polyvinyl alcohol (PVA) of 31000 g/mol average molecular weight. Zinc chloride powder (purified ZnCl2, purity 97%), was supplied from SDFCL-MUMBAI. Lab-scale glycerol with a purity of about 99% was supplied from Pubchem. Glutaraldehyde (GA)- solution 25% was supplied from LOBA CHEMIE- INDIA. These materials were similar as recommended by Kanagaraj et al. [41]

We purchased commercially available spiral wound modules applied as low-pressure reverse osmosis membranes. It was supplied from JOZZON Company-LTD for MEMBRANE TECHNOLOGY in China (REVERSE OSMOSIS ELEMENT) - JRW-1812-75-H for brackish water (desalination extended to 2000 ppm, operating pressure reached 10 bar). A4 sheets were cut for spiral RO-module which was opened stored for use as base membrane for prior modification. A flat sheet membrane 9 cm *6 cm (54 cm2 effective area) was used performance evaluation and the experiments were replicated for three times, averaged and presented.

2.2. Methodology

a Preparation and characterization of ZnO/Glycerolate nanocomposite

Firstly, $ZnCl_2$ -aqueous solution (80% by weight) was added to glycerol with a mole ratio of 1:1. Then sodium hydroxide solution (50% by weight) was introduced to $ZnCl_2$ and glycerol solution drop by drop under vigorous stirring at ambient temperature. The glycerol in this preparation method [42] acted as a template and stabilizer and plays an important role on prepared nanostructure morphology and size. The addition of sodium hydroxide was continued to reach

pH 12. Thereafter, the solution was stirred for further 5 minutes to complete the reaction. Then a white emulsion formed, which was thoroughly washed alternately with water and ethanol in several wash cycles to remove glycerol residues. The solid precipitate was separated by spinning for 10 minutes at 6000 rpm and after that dried in a furnace at 80°C for 10 hours. The received precipitate was then characterized using selected analytical techniques. We redeemed XRD (X-ray diffraction) analyses employing diffractometer with Cu-Ka radiation as Philips X'Pert Multipurpose Diffractometer [43]. The results were mean values after 5 readings. The images with Transmission electron microscopy (TEM) were obtained with a device from FEI-TECNAI T20 operated at 200 kV.

The chemical functional groups present in the Zn-nanocomposite of the fresh samples (undehydrated) were scanned using Fourier transform infrared spectroscopy (FTIR) technique. The analysis was fulfilled with a Bruker-Vertex70 FTIR/ OPUS software from Bruker Optics and using a detector of deuterated triglycine sulfate (DTGS) having accessory with attenuated total reflectance (ATR) and a Golden Gate diamond ranging from 4000 cm^{-1} to 600 cm^{-1} with resolution of 2 cm^{-1}, and error ±0.01 cm^{-1}. We performed TGA and DTG using Perkin-Elmer Diamond (TG/DTA). Thermogravimetric/differential thermal analyzer characterized nanostructure of zinc at temperature 1200°C of with a flowrate of 20°C/min .

b Chemical modification for RO membranes

Before layer deposition, commercial RO membrane samples were cut into A4 sheets where three groups were immersed in distilled water bath for a day to spill-off any preservative chemicals. Membrane modifications by chemical treatment expressed before in Jiang et al method [45]. The first group was composed of three A4 sheets for reproducibility and nominated MT31 which was the blank one (untreated), and the other three sheets nominated MT32 followed by the third group nominated MT33. The groups of MT32 and MT33 were impregnated in a (0.1%) by weight glutaraldehyde (GA) in deionized water at room temperature for about 12.0 h and then compassed dry in the air (2h). Chemical modification was then fulfilled with the deposition of PVA from its acidified solution in distilled water (0.1%) using an H_2SO_4 solution. Membranes MT32 was operated poly-fluor-tetra-ethylene (PTFE) frame, where membrane surface were subjected to PVA solution for 30 minutes for homogeneous deposition. Then, remaining solution was removed as membranes were left for drying in air for 2 minutes. After the crosslinking solution of 85% glutaraldehyde GA-solution in acetone was freshly prepared and then poured over the membrane surface for 90 minutes. Annealing for membranes were done in air oven for 5 minutes at 60°C. MT33 membranes were prepared by treatment with PVA solution in presence of Zn-nanocomposite (0.25%) which was dissolved in water with the same conditions as in MT32. Chemically- modified membranes MT32 and MT33 together with MT31 (blank one) were evaluated for salt rejection using a synthetic salt solution of from 1000 ppm to1050 ppm mixed salts of NaCl and $CaCl_2$ in distilled water and having ion concentration of 1000 ppm Na^+, 1040 ppm Cl^-, 20 ppm Ca^{++} The testing cell was composed of temperature-controlled feeding tank with a cross-flow- stainless steel cell with a high-pressure pump. We established experiments the at a constant pressure of 20 bar with 3 replicates.

c Irradiation modification of RO membranes

Vacuum ultraviolet(VUV) was used to treat A4 sheets commercial RO membrane using a traverse table and various modules for VUV . The effect membrane surface cleaning using ultrasonic waves was studied for bath exposure 1 min in deionized water [46]. In low-pressure mercury lamps (emission at 185 nm and 254 nm) only one lamp (Hönle: UVX 120 4C S 19/670 Co) was used. The distance between the outer surface of the lamp cylinder and RO membrane surface was 2 mm. Irradiation was performed under ambient air and room temperature. In all cases dependent on treatment speed, the temperature raised less than 30°C in low-pressure-mercury lamps and excimer lamps. Different treatment speeds of the traversing table were applied to vary the VUV radiation dosage.

2.3 Membrane characterization

Ultra-thin film was formed during surface coating over polyamide layer TFC- commercial RO membrane which been accomplished by cross-section scan with a top surface with scanning electron microscope (SEM) images- JEOL-5410 at 10,000V. FTIR- Fourier transform infrared- spectra using ThermoFisher Scientific Nicolet iS50) was used with 4 cm^{-1} spectrum resolution and this was very important to detect functional groups in membranes. The topographic images for membrane surface roughness and adhesion tests with AFM equipment were presented (Wet – SPM (Scanning Probe Microscope) Shimadzu). The quantitative nanomechanical (QNM) with a tapping mode in air was applied to samples (5 μm × 5 μm) membrane surface roughness and the nanomechanical and topographical images. We measured water contact angle of chemically modified membranes by using a compact mode, video microscope manufactured by SDL/UK and each value was averaged from 10 measurements. Pristine and VUV irradiated RO membranes contact angle were measured and the values were compared with published data for membranes with nearby polymeric structure and surface modification. The X-ray Photoelectron spectra were carried out for membranes to detect surface sensitively using VGESCALAB220i-XL using a monochromatic spectrometer Al-1486.6 eV X-ray source operated at 15000V and 20 milliampere. We averaged results of

two different measurements of each membrane sample.

2.4 Evaluation of modified RO membranes

We formulated relationships between operating parameters at different conditions of modified membranes. The evaluation was performed by measuring permeate flux and salt rejection described in equations 1 and 2, for feed solution 1000 ppm salinity with a testing cell having a membrane area 54 cm^2 and a pressure pump up to 20 bars and a feed solution tank capacity of 20 l. The saline feed solution was synthesised in these experiments by dissolving a mixed salt of NaCl and $CaCl_2$ having concentration of 1 gm/litre and 0.02 g/l respectively.

The permeability (J) was calculated as follows (1):

$$J = \frac{Q}{A \times \Delta t \times \Delta P} \quad (1)$$

where Q was permeate water mass in kilograms; A was the membrane active area in m^2, t was the time in an hour, and P was the operating pressure in bars.

We calculated the rejection (R) as (2):

$$\% R = \frac{(C_f - C_P) x\ 100}{C_f} \% \quad (2)$$

Where C_f = salt concentration in feed solution ,

C_p is the salt concentration in permeate.

2.5 Membrane chlorine resistance

A solution of sodium hypochlorite 8% by weight in distilled water was liquified dissolving corresponding to a free chlorine concentration of 0.46 g/l. We applied this solution for evaluation the polyamide layer stability in presence of PVA- RO membrane. The membranes (MT31, MT32, and MT33) were immersed in this solution for 24 hours in a sealed darkened vessel. The resulting membranes designated MT34, MT35, and MT36 respectively were evaluated after this artificial aging.

2.6 Membrane fouling testing

In experiments, we employed sodium alginate with humic acid as a model foulant. Initially, we measured the water permeability J_{w1} by brimming the distilled water through the membranes for 5 h . Further, the sodium alginate solution (1 g/l) mixed with (1 g/l) humic acid permeated through membranes for 5 h. The permeability of model foulant J_p (l/m^2 h/bar) was measured presuming the amount of produced water permeated from the membranes for 5 h. The fouled membranes were cleaned with distilled water for 30 min after removing of alginate/humic fouling solution. In the end, distilled water was streamed through membranes again for 5 h and measured the filtered water permeability J_{w2} (l/m^2 h/bar). The flux recovery ratio (FRR) was calculated as follows in eq (3):

$$FRR\ \% = \frac{J_{w2}}{J_{w1}} \cdot 100\% \quad (3)$$

We can determine reversible fouling ratio (R_r) and irreversible fouling ratio (R_{ir}) by the following equations (4, 5):

$$R_r\ \% = \frac{J_{w2} - J_p}{J_{w1}} \cdot 100\% \quad (4)$$

$$R_{ir}\ \% = \frac{J_{w1} - J_{w2}}{J_{w1}} \cdot 100\% \quad (5)$$

3. Results and discussions

3.1 Characterization of Zn containing precipitate

The prepared Zn-containing precipitate was subjected to XRD analysis, as shown in Figure 1. The presence of a distinguished peak at 11° and 17° was in conformity with published, [47] for zinc glycerolate while the peaks at 31°, 32°, 37°, and 59° were assigned to ZnO nanoparticles following [48,49].

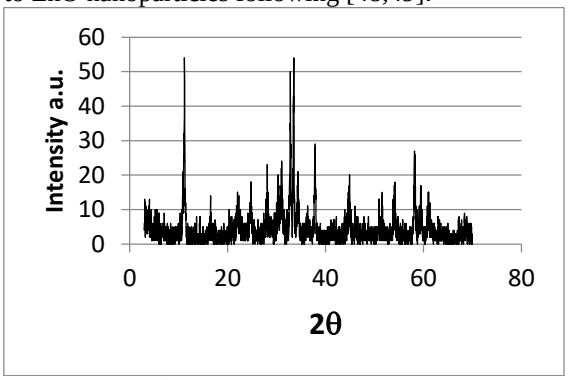

Fig. 1. XRD- plot for obtained Zn nanocomposites

In Figure 2, appearances of strong and broad absorption bands were registered in the region of 3600 cm^{-1} to 3000 cm^{-1} and a slightly small absorption band from 1650 cm^{-1}- 1600 cm^{-1}. The bands absorbed were assigned to stretching and bending vibration modes of the free hydroxyl group. This indicated the presence of water or unreacted free glycerol in the precipitate. The two strong and sharp absorption bands at 2980 cm^{-1} and 2934 cm^{-1} were due to C-H stretching vibration modes and specifically for C–H stretching vibrations of CH_2 and CH_3 groups respectively. The sharp absorption bands that occurred between 1120 cm^{-1} and 904 cm^{-1} were assigned to the C-O bending modes of alcohol present in the precipitate. In addition, the peaks at 1073 cm^{-1} and 1623 cm^{-1} were attributed to stretching vibrations of the C–O and C=O bonds. Absorptions region from 1300 cm^{-1} to 850 cm^{-1} is sensitive for complex interacting vibrations, causing a rise generally to a unique fingerprint for every compound. The fingerprint region was interpreted as similar to that of glycerol [42].

The absorption bands below 550 cm^{-1} were assigned to metal-ligand complexes which in this case indicated the zinc glycerolate with ZnO nanoparticles forming organo-metallic complex but for the peak at 713 cm^{-1}, it was attributed to the presence of a trace amount of ester from glycerol [48,49].

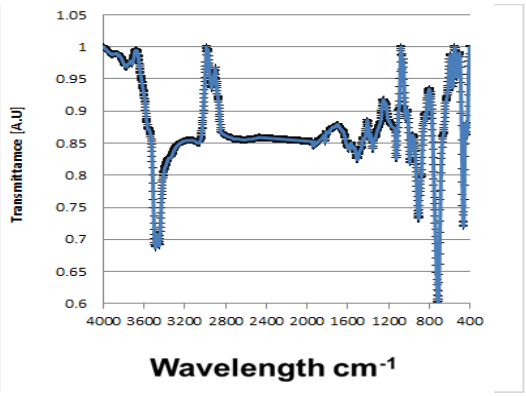

Fig 2. FTIR plot for Zn-glycerolate complex

The curves in Figure 3 showed that the decomposition reaction occurred in two well-defined steps. The first step occurred at temperatures between 160°C and 238°C with a weight loss of 16.04%, accompanied by an asymmetric endothermic peak observed in this temperature range (T_{max} = 200°C). This peak was assigned to the loss of glycerol. A second decomposition step was observed at temperatures between 360°C and 600°C with a weight loss of about 25%, accompanied by a peak in DTG at 540°C. This decomposition step was assigned to dehydration and a loss of water.

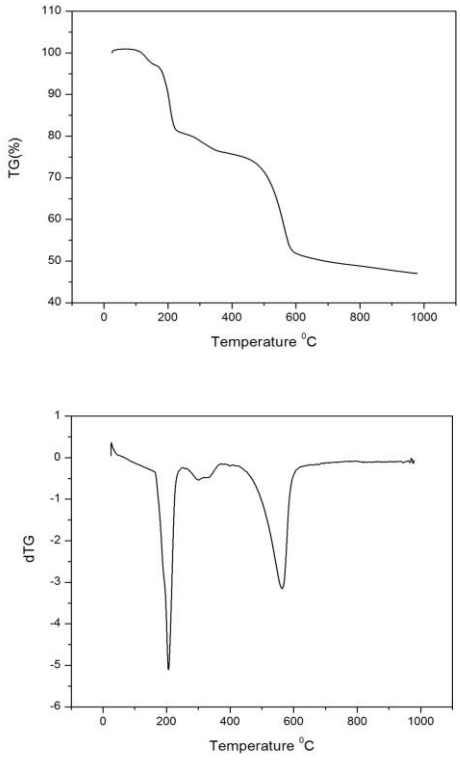

Fig. 3. TGA and dTG of precipitate ZnO /Zn-glycerolate nanostructure

Finally at a temperature of 602°C TG and DTG curves stabilized yielding a residue of ZnO, with an overall experimental weight loss of 18.088 less than reported in the literature [50]. The little weight loss was due to the role of glycerol in the stabilization of ZnO nanoparticles formed from $ZnCl_2$, a hygroscopic metal halide.

The presence of ZnO nanorods was enveloped with zinc glycerolate nano-blanket as shown in the TEM plot -Figure 4. This plot showed the presence of both structures as the shape of some amorphous phase structure.

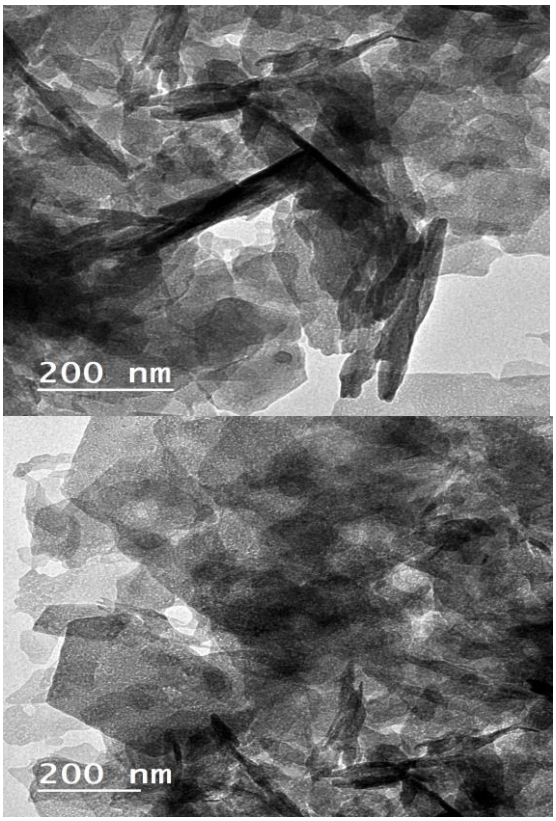

Fig 4. Transmitting Electron Microscope (TEM) of Zn-containing precipitate with/without PVA)

Because of the aforementioned results, the Zn-containing precipitate consisted of Zn-glycerolate and ZnO particles. These particles consisted of agglomerated nanoparticles with various particle shapes.

3.2 Characterization of chemically modified membranes

a Contact angle

The effect of the chemically deposited PVA layer was examined in the presence of a chlorine-containing solution to govern its stability as shown in Figure 5. The contact angle showing the hydrophilic property of chemically modified TFC RO membranes was presented in Figure 5. In presence of Zn - nanocomposite in the PVA layer for membranes MT33, which exposed a high enhancement for hydrophilicity to reach a contact angle of 10°C**.** This value demonstrated a dramatic increase to reach 45°C for MT36 which meant that the presence of Zn nanostructure damaged the PVA layer when compared

with MT32. PVA stabilized the nature of the deposited layer in presence of chlorine at MT35.

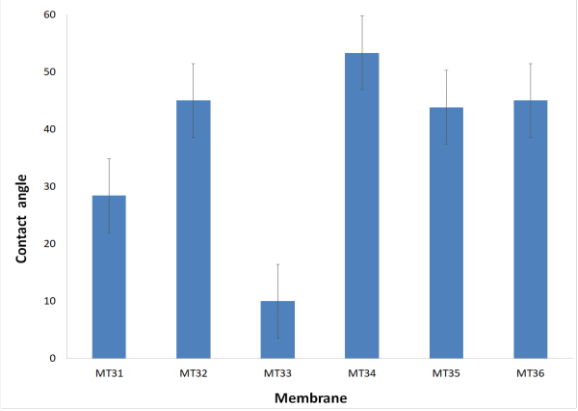

Fig. 5. Contact angle variation for RO membranes with chlorine exposure

b AFM morphology

Commercial membrane MT31 and chemically modified ones MT32, and MT33 were examined for surface roughness measured that demonstrated the influence of the presence of Zn nanostructure in the deposited layer.

It was clearly shown in Figure 6 that MT31 membranes exhibited the major dark spots, indicated a rougher surface, and contained a large number of pores with the highest height of peaks indicating roughness. The pores size of MT33 was smaller and lowered roughness when compared to MT32 and MT31. MT33 was least fouled with sodium alginate/humic acid (polysaccharide) as it exhibited the major bright spots. Those spots indicated higher absorption of solutes on its surface, therefore, leading to severe fouling.

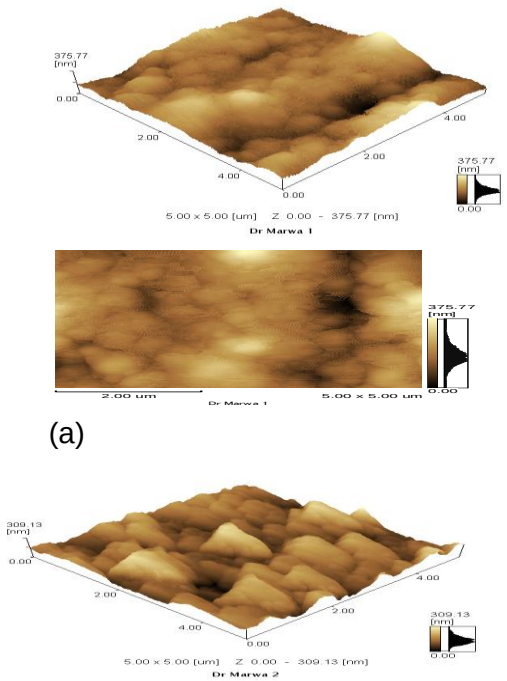

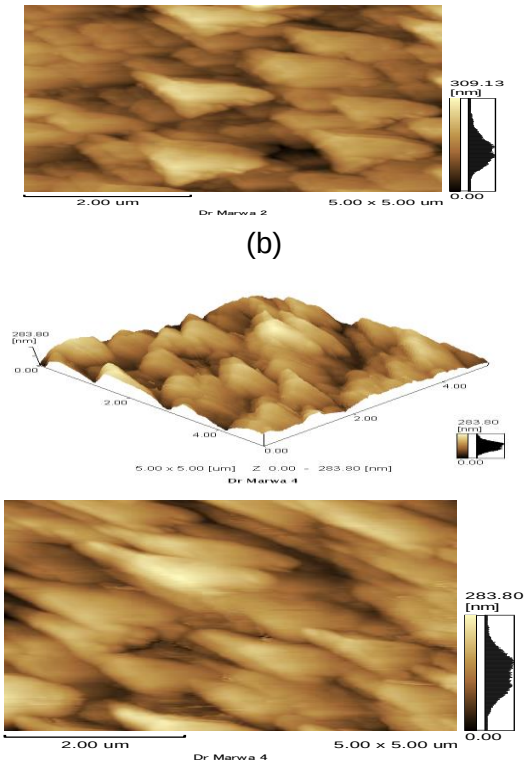

Fig. 6. AFM morphology of membranes MT31(a), MT32 (b) and MT33(c)

3.3 Chlorine resistance – RO membrane performance

The salt rejection attained by RO-membranes together with water permeability with exposure to chlorine and without were recorded and shown in Figure 7 and Figure 8 as MT31 which was "the commercial blank". MT32, the one coated with PVA and compared to MT33 showed the effect of the ZnO/PVA coated layer. The effect of chlorine aging on the commercial blank was MT34, while MT35 was the one that aged after having a PVA layer, and finally, the presence of Zn oxide -glycerolate upon aging was shown in MT36 ➔ PVA/Zn. It was evident from reached data that the percent rejection was highly enhanced. This growth was caused by the presence of a protective dense layer of PVA cross-linked with the polyamide layer which enhanced it and this was clear for MT32 and MT33. But after exposure to chlorine, it was found that permeability was affected dramatically and showed the worst adverse effect of chlorine on MT31. The membrane permeability was highly increased as if it was pitted but the rejection was not affected as a primary stage as shown in the SEM plot (Figure 9). In the same circumstances of membranes soaking, MT32 and MT33 with extra PVA deposited layer showed some barrier as MT33 The MT33 was better as the permeability showed a little increase, less than at MT32 where the permeability reached 14.2 LMH/bar.

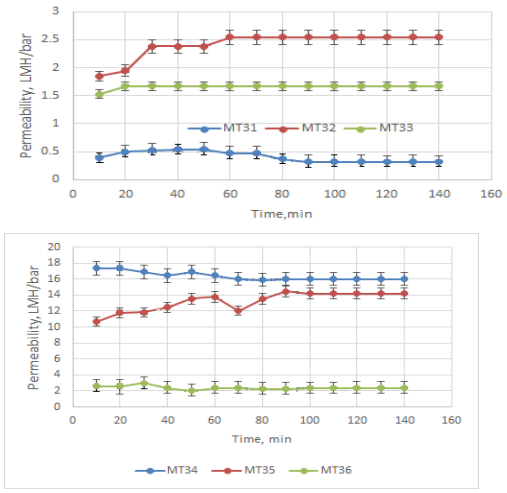

Fig. 7. RO-membranes permeability with/without chlorine

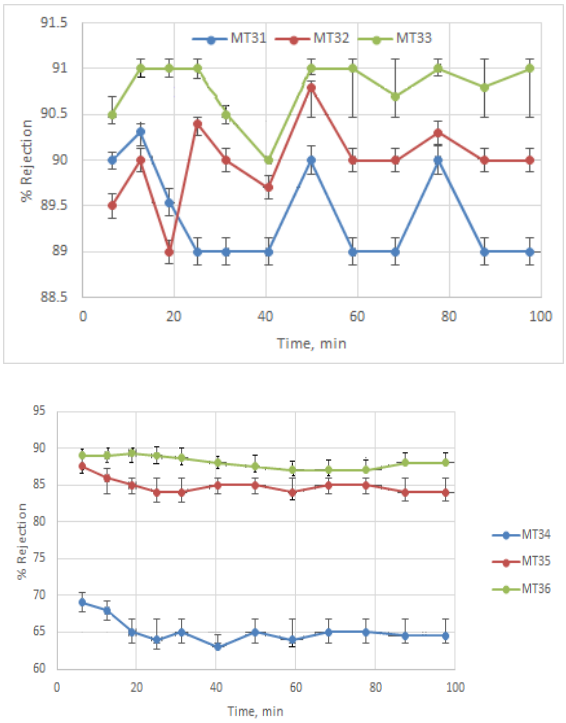

Fig. 8. RO-membranes rejection with/without chlorine

Figure 9. indicated the top and cross-section of M31 before soaking in chlorine and M34 after soaking in chlorine, where the dense layer appeared on the cross-section of M31. The top surface indicated the appearance of crosslinking polymerization as a net of polymeric chains, due to the formation of a polyamide layer as shown in Figure 9a. On the other hand, M34 top surface indicated the net structure of the polyamide layer disappeared. The cross-section of this membrane indicated a reduction in the top thin layer and deformation in the membrane sublayer as shown in Figure 9b.

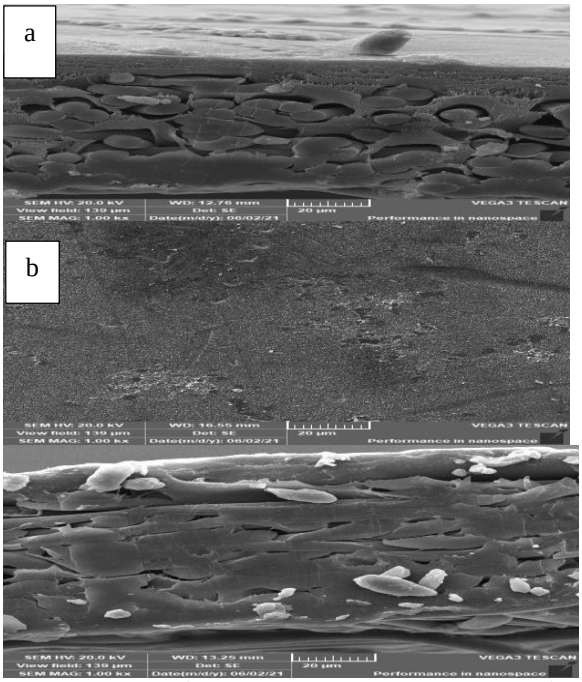

Fig. 9. SEM plot for MT31-top and cross-section (a) before exposure to chlorine and (b) MT34 after its exposure

Figure 10 indicated the top and cross-section of M32 before soaking in chlorine and M35 after soaking in chlorine. The top surface of M32 demonstrated a covered layer of the polyamide layer where the net structure disappeared, and the cross-section illustrated a highly thick layer of polyvinyl alcohol (PVA) coating layer. This thick layer was due to the covalent bond between PVA and the polymeric chain in the polyamide layer, which provided to improve the physic-chemical properties of the membrane surface [51].

After soaking in chlorine M35 image exhibited that the PVA layer resisted the chlorine and the thick dense top layer still appeared. This was due to the covalent linkage of PVA molecules with the amino groups' sites and amide linkages (–CONH–), which produced a protective coating layer and prevented the attack of chlorine on the underlying thin film layer [51].

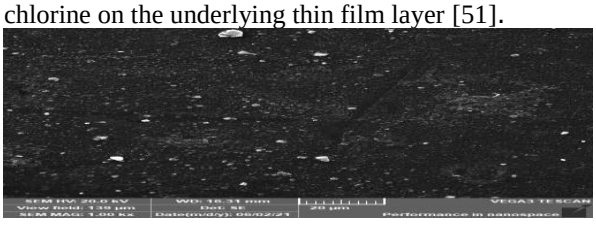

a

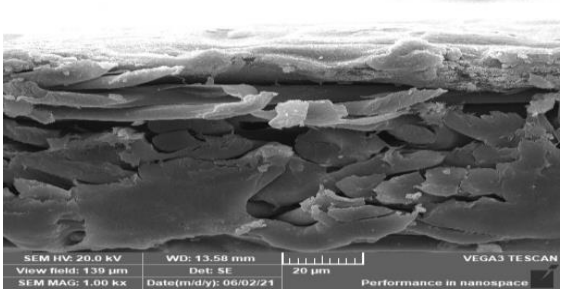

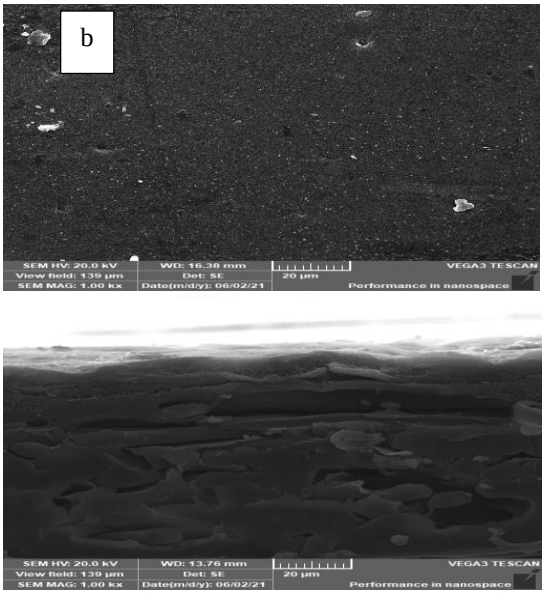

Fig. 10. SEM plot for MT32-top and cross-section (a) before exposure to chlorine and (b) MT35 after its exposure

Figure 11. indicated top and cross-section of M33 before soaking in chlorine and M36 after soaking in chlorine. The top surface of M33 exhibited a top dense layer with an absence of net structure of polyamide layer due to the coating by PVA, using zinc oxide as a nanoparticle on the coating layer of PVA exposed rough surface. After soaking in chlorine, M36 indicated no change in the top dense layer which meant using PVA with ZnO in the coating layer provided a highly efficient layer to resist chlorine.

Soaking the membrane in chorine solution reduced the C-N ratio, by the substitution of N-H in the amide group with N-Cl by the free chlorine. Applying zinc oxide in the PVA layer protected a C-N ratio due to saving the polyamide layer by a reaction of free chlorine with ZnO to form Zn-Cl bonding on the surface as an alternative to N-Cl [52].

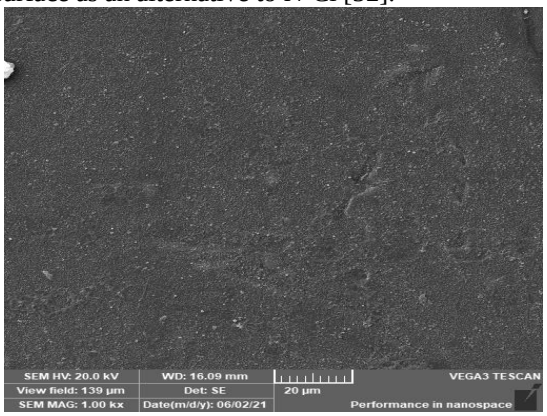

a)

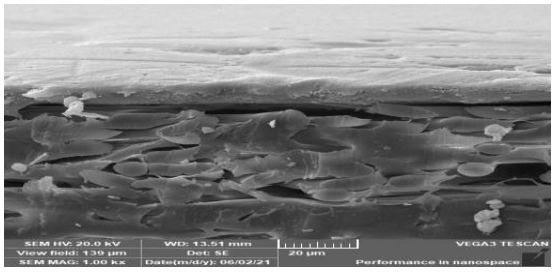

b)

Fig. 11. SEM plot for MT33-top and cross-section (a) before exposure to chlorine and (b) MT36 after its exposure

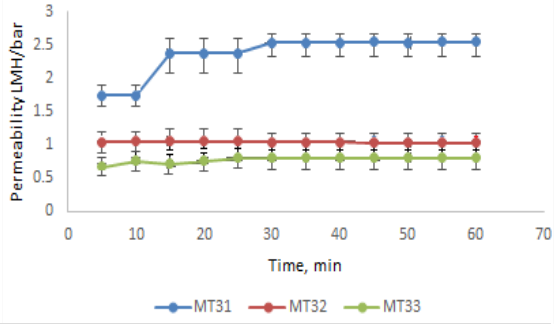

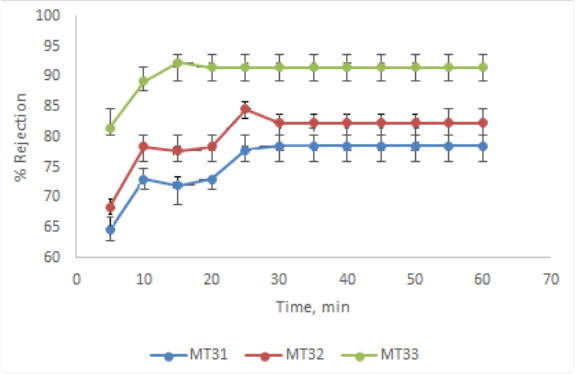

Fig. 12. Rejection % and permeability at chlorine concentration 0.26 g/l with synthetic salt solution

By changing the concentration of free chlorine in feed synthetic saline water (from 0.26 to 0.46 g/l), the performance of membranes was compared as shown in Figures 12 and 13. One can notice easily the difference in achieved % rejection was the highest at MT33 with 91%±6% at 0.46 g/l chlorine and 83% respectively. For the permeability, it was increasing with the chlorine attack for MT31 but for MT33 it was withstanding and showed lower values.

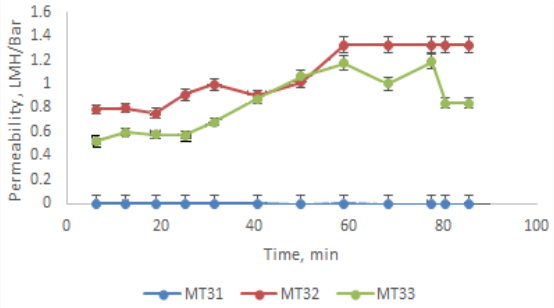

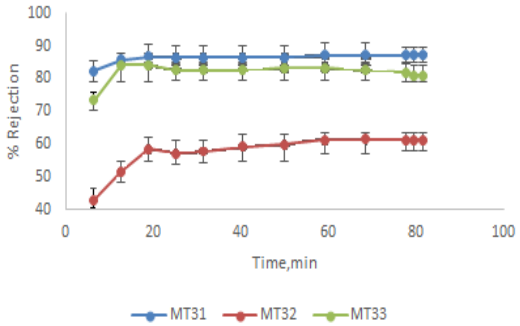

Fig. 13. RO-permeability and % rejection at chlorine concentration 0.46 g/l with synthetic salt solution

3.4 Performance study for antifouling behavior

The fouling experiment (Figure 14) was verified using sodium alginate as a model polysaccharide/humic foulant for membranes MT31, MT32, and MT33 as expressed above. It was clear that surface modification of membranes using PVA/GA in presence of Zn nanocomposite (MT33) showed better anti-fouling behavior as shown in Table 1 but needed further enhancement to decrease the percent of irreversible fouling [53].

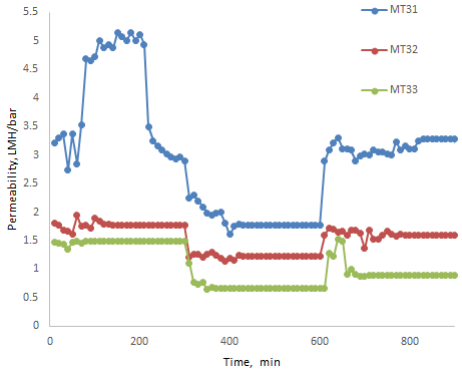

Fig. 14. Fouling experiment for modified RO membranes

Antifouling behavior was precisely evaluated on comparison with published data[1,22] as shown in Table 1, where the maximum reached about 91% the same as our study which showed about 90%.

Table 1.
Fouling indicators for selected membranes.

No	MT33	MT32	MT31
%FRR	59.59%	89.90%	60%
%Rr	14.68%	20%	25%
%Rir	42.76%	10.48%	40%

3.5 RO-Performance for Vacuum UV irradiation

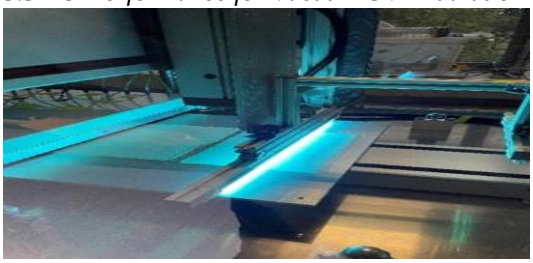

Fig. 15. Activation of PA-TFC RO membranes using vacuum UV device

The exposure rate and intensity of the vacuum UV radiation (Figure. 15) were varied to show its effect on the hydrophilicity of the RO membrane. The measurement of the water contact angle showed that the hydrophilicity extended with the increase of applied vacuum UV dosage. Even at web speeds of 30 m/min, the water contact angle was curtailed from 76° in pristine TFC-RO membrane to 53° after vacuum UV irradiation.

The detailed results of the water contact angles depending on the treatment speed and the types of VUV lamps used were shown in Figure 16.

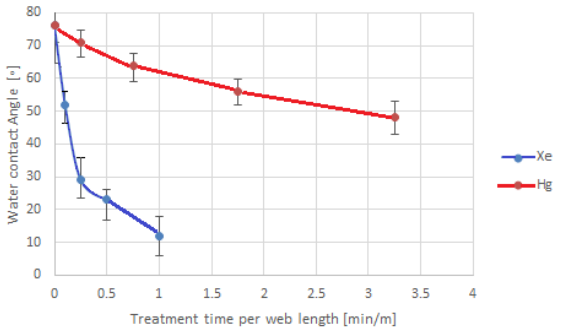

Fig 16. Water contact angle after various VUV treatments: variation of treatment speed and radiation source (low-pressure Hg-lamp and Xe-excimer lamp)

This behavior proved the activation effect of vacuum UV irradiation at 172 nm (excimer lamps) and 184 nm (low-pressure Hg lamps). The increase in hydrophilicity through VUV treatment meant that improved fouling behavior could be expected.

Taking the different number of lamps and different emission strengths of lamps into account treatment with 1 m/min with an excimer lamp module and treatment with 3.3 m/min Hg-lamp resulted in a similarly applied vacuum UV dosage. A direct comparison of these treatments showed tremendous differences in water contact angle: 12° in the case of Xe-excimer lamps and 48° in the case of Hg lamps. Therefore, it was indicated that the activation effect of VUV radiation at 172 nm was stronger than at 184 nm. This was assigned to stronger absorption of VUV radiation with smaller wavelengths which was typical for organic substances. Concerning water contact angle the samples Hg 3.3 and Xe 1 were comparable with the chemically modified sample MT32 and the sample Xe 0.1 with MT33.

a SEM Characterization of VUV-Irradiated membranes

Figure 17 illustrated the modified membrane M31 surface using VUV irradiation with a web speed of 1 m/min. Where, Figure (17 a) indicated that the top surface of the modified membrane by VUV irradiation with this dose did not damage the polyamide layer. There the net structure of the cross-linked polymerization reaction appeared clearly on the

surface. Also, the cross-section of this membrane indicated the formation of more dense zones on the surface, which meant the treatment using 1 ml/min provided a wavey shape of the membrane surface, which could lead to a thick dense layer in some places in the surface and low dense layer in other places in the surface as shown in cross-section Figures (17b and 17c).

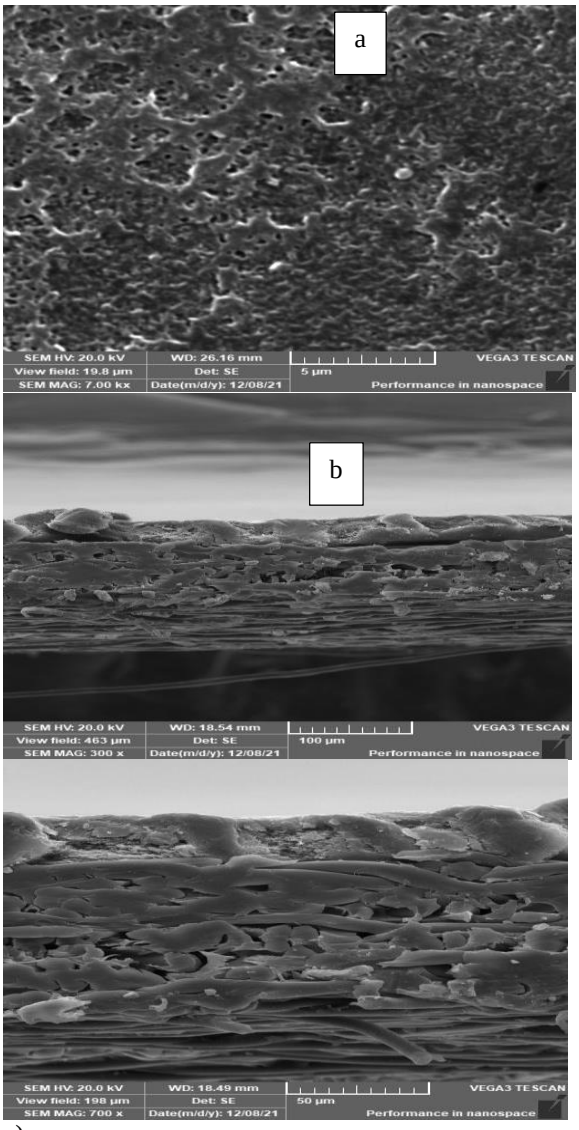

c).

Fig 17. SEM morphology for irradiated membranes VUV 1 m/min

Figure 18. illustrated the modified membrane surface using Hg 0.3 m/min. The top surface image indicated the disappearance of the polyamide thin film layer or a reduction in the size of the polymerization crosslinked net. Thus meant the dense structure of the surface was reduced as shown in Figures (18 b and 18 c), where the cross-section images indicated a low wavey shape.

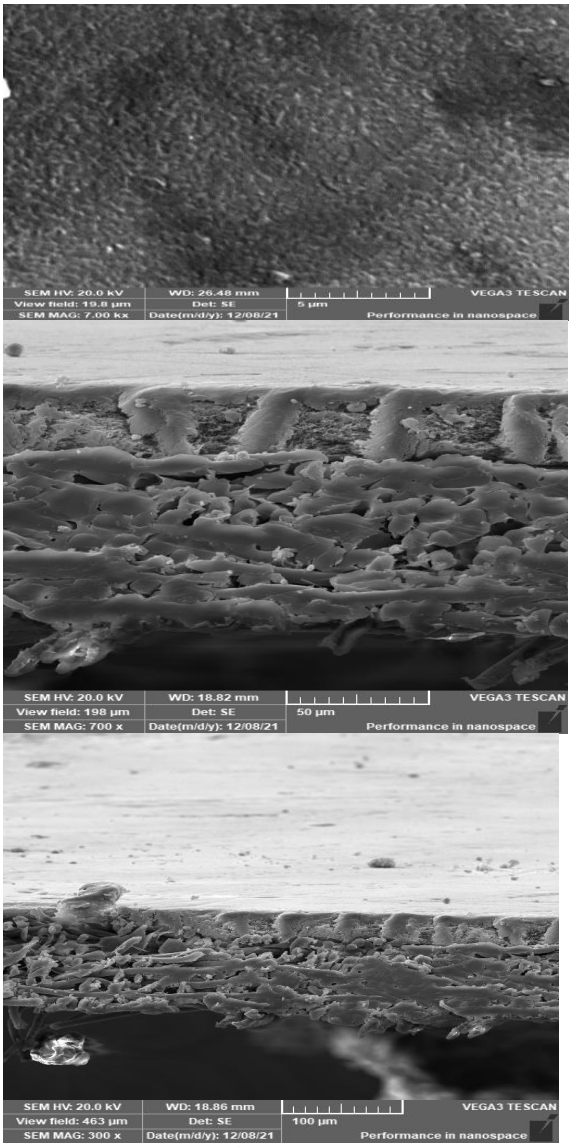

Fig. 18. SEM morphology for irradiated membranes Hg 0.3 m/min

Figure 19. illustrated the images of the membrane M31 after ultrasonic cleaning which indicated the damage of the polyamide layer due to the formation of large voids on the surface (see Figure. 19a). However, the cross-section images (b and c) indicated a smooth surface with to reduction in the thickness of a dense layer, which indicated dense layer deformation.

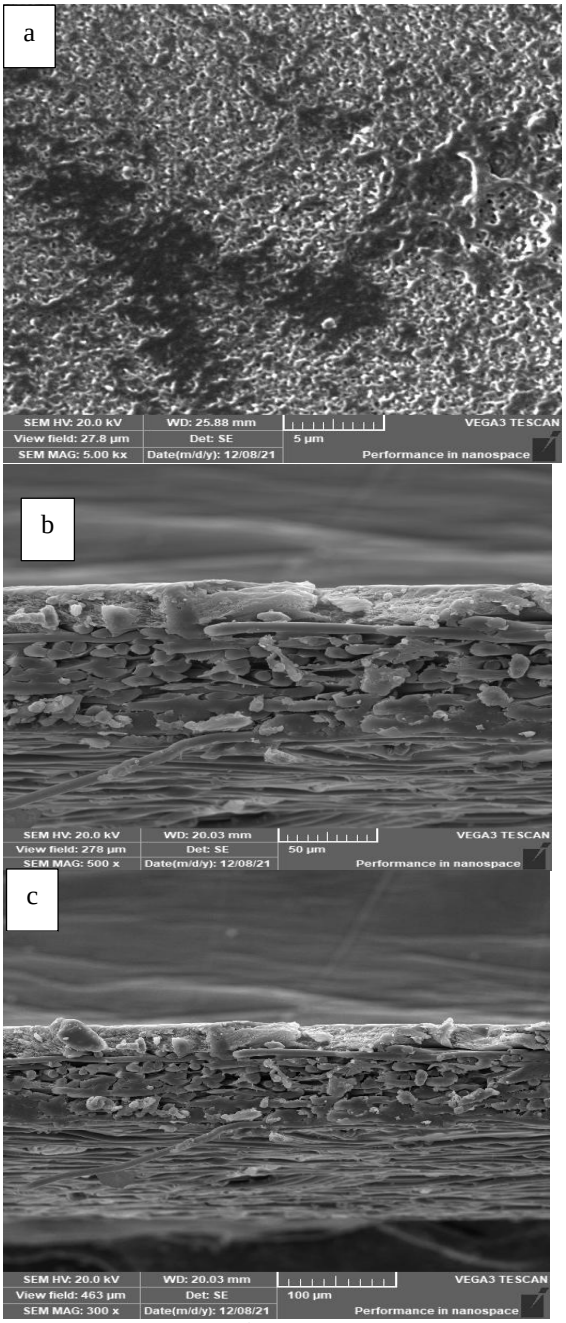

Fig. 19. SEM morphology for irradiated membranes US cleaning 0.3 m/min.

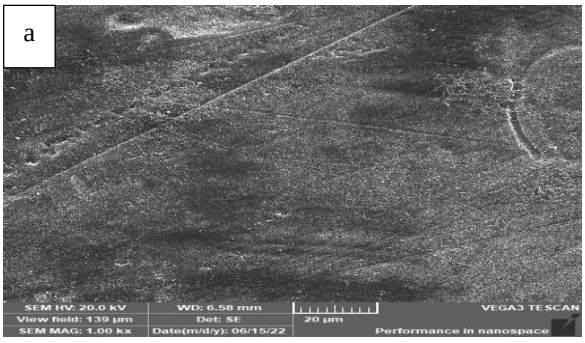

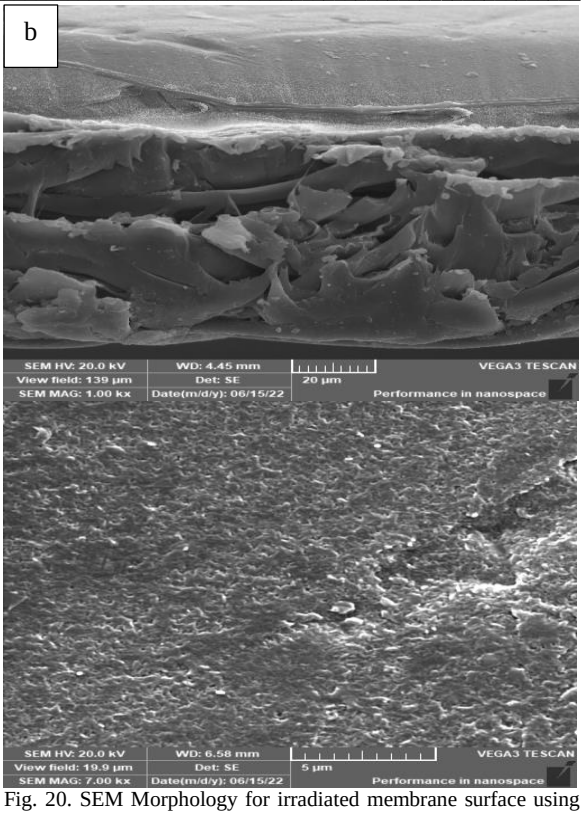

Fig. 20. SEM Morphology for irradiated membrane surface using VUV 10 m/min.

The top surface image indicated a slight change in the polyamide thin film layer top surface Figure 20a, which meant the dense structure of the top surface as displayed in Figure 20b. Figures. 20 showed an interaction between VUV at higher web speed and realized better surface treatment.

3.6.-XPS-studies of activated polyamide RO membrane (without and with water cleaning)

The comparison was held and measured at two positions one with water cleaning before activation and the other without water cleaning as shown in Tables 2. and 3.

The activation effect of vacuum UV irradiation was also supported by the characterization of the elemental composition of the surface by X-ray photoelectron spectroscopy.

Tables 2. and 3. compared a peak position of a polyamide-based, commercial RO membrane with the same oxygen and nitrogen concentration. Furthermore, a presence of alcohol/ether species was present, therefore the surface of the TFC RO membrane was modified.

Because ethers/alcohol and carbonyl and a slight amount of carboxyl were detected also after ultrasonic cleaning in water the commercial TFC RO membranes were probably plasma treated.

.

Table 2. Elemental composition of TFC RO-membrane surfaces after vacuum UV irradiation and ultrasonic cleaning, irradiations in the air at a distance of 2 mm (XPS measurements)

Sample name	**C %**	**O %**	**N %**	**Si %**	**S %**	**Cl %**	**Na %**	**Ca %**	**Al %**
Pristine TFC RO-membrane	66.2	27.1	5.2	0.2	0.3	0.3	0.7	-	-
US bath	69.7	22.4	6.9	0.2	0.3	0.3	-	-	0.3
US bath + Hg 0.3 m/min	68.1	26.3	5.0	0.2	0.3	0.3	-	0.2	-
Hg 0.3 m/min	67.4	28	3.35	0.25	0.3	0.25	0.45	-	-
VUV 10 m/min	62.7	28.7	7.1	0.1	0.3	0.3	1.0	-	-
VUV 1 m/min	66.5	26.,1	6.0	0.1	0.3	0.4	0.8	-	-

Table 3. Chemical composition of TFC RO-membrane surfaces after vacuum UV irradiation and ultrasonic cleaning, irradiations in the air at a distance of 2 mm (XPS measurement of C1s-photoline and peak fit)

Sample name	Peak position 285.0 eV [%]	Peak position 286.5 eV [%]	Peak position 287.2 eV [%]	Peak position 289.5 eV [%]
Reference	52.05	42.15	5.6	0.15
Reference (ultrasonic cleaning)	61.4	29	9.45	0.2
Hg 0.3 m/min (ultrasonic cleaning)	54.85	33.6	10.05	1.5
Hg 0.3 m/min	51.3	38.85	9.05	0.8
VUV 10 m/min	46.6	34.2	17.05	2.15
VUV 1 m/min	51.65	37.4	10.35	0.7

The effect of US cleaning decreased the amount of ether/alcohol and led to the removal of loosely bound components which were probably low molecular weight components. VUV treatment after cleaning increased oxidized species (ether/alcohols + carbonyl + carboxylic) and this was a sign of activation by VUV irradiation.

VUV treatment without prior cleaning decreased alcohol/ether (degradation and oxidation of alcohol to higher oxidized species) which increased carbonyl groups and carboxylic groups as a sign of activation.

High dosages provided a high amount of oxidized species and caused surface deformation which damaged effect flux and salt rejection. If the membrane was cleaned by an ultrasonic bath before irradiation the TFC RO membrane was partly damaged by the ultrasonic cleaning, because the retention flux was increased tremendously as shown in SEM morphology Figures. 17-20.

3.7. Performance Evaluation for VUV-Irradiation

Desalination tests of irradiated samples of PA-TFC membranes were fulfilled using the lab-scale cell previously illustrated.

The synthetic salinated water in the range from 970 ppm to 1070 ppm was prepared using mixed NaCl and $CaCl_2$. The effect of VUV irradiation on PA-TFC membranes was studied and recorded in Figures 21 and 22.

In the case of Hg-lamp irradiation (0.3 m/min) the salt rejection, and the permeate flux, were slightly changed compared to the commercial TFC RO membrane. More aggressive irradiation by the Xe excimer lamp module at 10 m/min increased the permeate flux by about 20% but decreased the salt rejection from 87% to 62%.

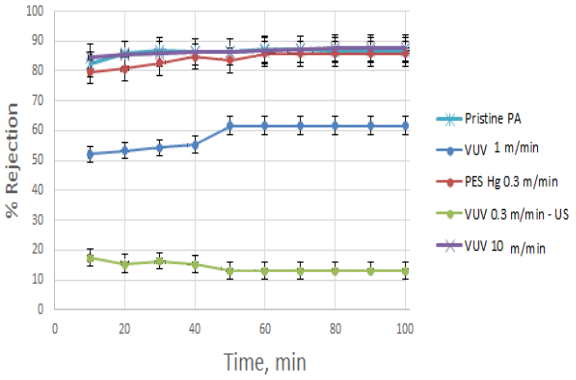

Fig. 21. Salt rejection of RO-membrane in dependence on surface modification and permeation time

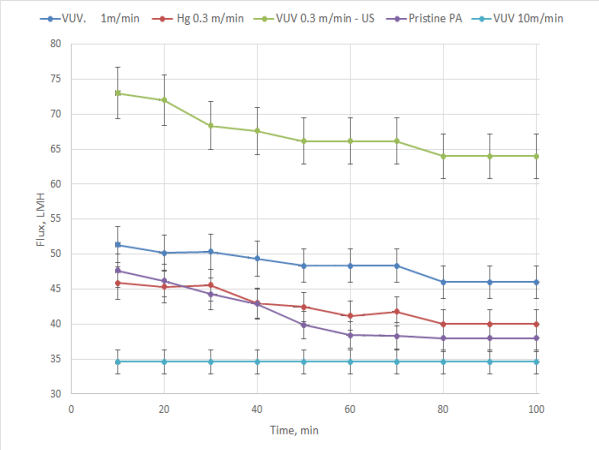

Fig. 22. Permeate flux of RO-membrane in dependence on surface modification and permeation time

Because the activation effect was accompanied by an etching effect, the TFC RO membrane was probably slightly deteriorated already. For VUV 10 m/min the salt rejection was increased to reach 87% the same as

Hg lamp activation and pristine membranes but the flux for VUV 10 m/min. It decreased to reach 35 LMH when compared to a Hg lamp of about 40 LMH.

4. CONCLUSIONS

The exposure to chlorine highly affected the surface of membranes but the presence of Zn nanostructures embedded in the PVA/GA layer highly enhanced the performance concerning fouling behavior and flux recovery ratio. Treatment of TFC membrane surface highly enhanced surface hydrophilicity to show a contact angle of 8.7° at optimized web speed. The minimum contact angle reached with the chemical deposition layer of PVA was determined as 10° and attributed to the presence of ZnO nanostructure with Zn-glycerolate.

Membranes MT31 as the blank TFC, and the other two MT32, MT33 which were modified by PVA in the absence and presence of Zn-nanocomposite (0.25% by Wt) dissolved in water respectively (i.e. PVA + GA & PVA + Zn nanocomposite (0.25%)+GA respectively. The application of VUV irradiation on commercial TFC membranes highly influenced its behavior in terms of permeate flux and salt rejection. We detected the highest irradiation Hg 0.3 m/min as it increased % salt rejection to reach 87% and flux permeation of about 40 LMH. This was in addition to the adverse effect shown by ultrasonic water bath cleaning which caused a serious deterioration in the TFC-polyamide layer reflected upon reaching flux and salt rejection.

5. Conflicts of interest

There are no conflicts to declare

6. Formatting of funding sources

This work was kindly funded and supported through Science, Technology &Innovation Funding Authority (STIFA) in EGYPT as a GERF call - Cycle 5 ID number 33633 and BMBF from Bremen-GERMANY.

7. Acknowledgments

This work was kindly funded and supported through Science, Technology &Innovation Funding Authority (STIFA) in EGYPT as a GERF call - Cycle 5 ID number 33633 and BMBF from Bremen-GERMANY).

8. References

1. Xie L, Liu Y, Zhang W, Xu S (2021) A dopamine/tannic-acid-based co-deposition combined with phytic acid modification to enhance the anti-fouling property of RO membrane. Membranes (Basel). doi: 10.3390/membranes11050342
2. Al-Gamal AQ, Saleh TA, Alghunaimi FI (2022) Nanofiltration membrane with high flux and oil rejection using graphene oxide/β-cyclodextrin for produced water reuse. Mater Today Commun 31:103438. doi: 10.1016/J.MTCOMM.2022.103438
3. Abdallah H, El Gendi A, Shalaby MS, et al (2018) Influence of cellulose acetate polymer proportion on the fabrication of polyvinylchloride reverse osmosis blend membrane, experimental design. Desalin Water Treat 116:29–38. doi: 10.5004/dwt.2018.22306
4. Yamamoto K (2022) Development of reverse osmosis membranes by incorporating polyhedral oligomeric silsesquioxanes (POSSs). Polym J. doi: 10.1038/s41428-022-00668-2
5. Keeling CI, Ngo HT, Benusic KD, Slessor KN (2001) Preparative chiral liquid chromatography for enantiomeric separation of pheromones. J Chem Ecol 27:487–97.
6. Sharma PR, Sharma SK, Lindström T, Hsiao BS (2020) Nanocellulose-Enabled Membranes for Water Purification: Perspectives. Adv Sustain Syst 4:1900114. doi: https://doi.org/10.1002/adsu.201900114
7. Lau WJ, Ismail AF, Misdan N, Kassim MA (2012) A recent progress in thin film composite membrane: A review. Desalination 287:190–199. doi: 10.1016/j.desal.2011.04.004
8. Yadav D, Karki S, Ingole PG (2022) Current advances and opportunities in the development of nanofiltration (NF) membranes in the area of wastewater treatment, water desalination, biotechnological and pharmaceutical applications. J Environ Chem Eng 10:108109. doi: https://doi.org/10.1016/j.jece.2022.108109
9. Yang Z, Zhou Y, Feng Z, et al (2019) A review on reverse osmosis and nanofiltration membranes for water purification. Polymers (Basel) 11:1–22. doi: 10.3390/polym11081252
10. Amakiri KT, Ogolo NA, Angelis-Dimakis A, Albert O (2022) Physicochemical assessment and treatment of produced water: A case study in Niger delta Nigeria. Pet Res. doi: https://doi.org/10.1016/j.ptlrs.2022.05.003
11. Lavelli V, Beccalli MP (2022) Cheese whey recycling in the perspective of the circular economy: Modeling processes and the supply chain to design the involvement of the small and medium enterprises. Trends Food Sci Technol. doi: https://doi.org/10.1016/j.tifs.2022.06.013
12. Riquelme C, Gómez G, Vidal G, Neumann P (2022) Critical analysis of the performance of pilot and industrial scale technologies for sewage reuse. J Environ Chem Eng 108198. doi: https://doi.org/10.1016/j.jece.2022.108198
13. Moyo S, Makhanya BP, Zwane PE (2022) Use of bacterial isolates in the treatment of textile dye wastewater: A review. Heliyon 8:e09632. doi: https://doi.org/10.1016/j.heliyon.2022.e09632
14. Abejón R (2022) A Bibliometric Analysis of Research on Selenium in Drinking Water during the 1990–2021 Period: Treatment Options for Selenium Removal. Int J Environ Res Public Heal . doi: 10.3390/ijerph19105834
15. Ren B, Weitzel KA, Duan X, et al (2022) A comprehensive review on algae removal and control by coagulation-based processes:

mechanism, material, and application. Sep Purif Technol 293:121106. doi: https://doi.org/10.1016/j.seppur.2022.121106
16. La YH, Sooriyakumaran R, Miller DC, et al (2010) Novel thin film composite membrane containing ionizable hydrophobes: PH-dependent reverse osmosis behavior and improved chlorine resistance. J Mater Chem 20:4615–4620. doi: 10.1039/b925270c
17. Gohil JM, Suresh AK (2017) Chlorine attack on reverse osmosis membranes: Mechanisms and mitigation strategies. J Memb Sci 541:108–126. doi: 10.1016/j.memsci.2017.06.092
18. Lasisi KH, Ajibade TF, Zhang K (2022) Degradation impact of low pH mineral acids and long exposure period on the active layer of semi-aromatic polyamine-based nanofiltration membrane. Polym Degrad Stab 200:109941. doi: https://doi.org/10.1016/j.polymdegradstab.2022.109941
19. Panagopoulos A, Giannika V (2022) Comparative techno-economic and environmental analysis of minimal liquid discharge (MLD) and zero liquid discharge (ZLD) desalination systems for seawater brine treatment and valorization. Sustain Energy Technol Assessments 53:102477. doi: https://doi.org/10.1016/j.seta.2022.102477
20. Panagopoulos A (2022) Techno-economic assessment and feasibility study of a zero liquid discharge (ZLD) desalination hybrid system in the Eastern Mediterranean. Chem Eng Process - Process Intensif 178:109029. doi: https://doi.org/10.1016/j.cep.2022.109029
21. Dahiru UH, Saleem F, Al-sudani FT, et al (2022) Oxidative removal of hexane from the gas stream by dielectric barrier discharge reactor and effect of gas environment. Chem Eng Process - Process Intensif 178:109035. doi: https://doi.org/10.1016/j.cep.2022.109035
22. Liu M, Chen Q, Wang L, et al (2015) Improving fouling resistance and chlorine stability of aromatic polyamide thin-film composite RO membrane by surface grafting of polyvinyl alcohol (PVA). Desalination 367:11–20. doi: 10.1016/J.DESAL.2015.03.028
23. Zirehpour A, Rahimpour A, Arabi Shamsabadi A, et al (2017) Mitigation of Thin-Film Composite Membrane Biofouling via Immobilizing Nano-Sized Biocidal Reservoirs in the Membrane Active Layer. Environ Sci Technol 51:5511–5522. doi: 10.1021/acs.est.7b00782
24. Yin J, Kim E-S, Yang J, Deng B (2012) Fabrication of a novel thin-film nanocomposite (TFN) membrane containing MCM-41 silica nanoparticles (NPs) for water purification. J Memb Sci 423–424:238–246. doi: https://doi.org/10.1016/j.memsci.2012.08.020
25. Xiong S, Xu S, Phommachanh A, et al (2019) Versatile Surface Modification of TFC Membrane by Layer-by-Layer Assembly of Phytic Acid–Metal Complexes for Comprehensively Enhanced FO Performance. Environ Sci Technol 53:3331–3341. doi: 10.1021/acs.est.8b06628
26. Deng E, Chen X, Rub D, et al (2022) Energy-efficient membranes for microalgae dewatering: Fouling challenges and mitigation strategies. Sep Purif Technol 296:121382. doi: https://doi.org/10.1016/j.seppur.2022.121382
27. Esfahani MR, Aktij SA, Dabaghian Z, et al (2019) Nanocomposite membranes for water separation and purification: Fabrication, modification, and applications. Sep Purif Technol 213:465–499. doi: 10.1016/j.seppur.2018.12.050
28. Douglass M, Garren M, Devine R, et al (2022) Bio-inspired hemocompatible surface modifications for biomedical applications. Prog Mater Sci 130:100997. doi: https://doi.org/10.1016/j.pmatsci.2022.100997
29. Ma R, Lu X, Zhang S, et al (2022) Constructing discontinuous silicon-island structure with low surface energy based on the responsiveness of hydrophilic layers to improve the anti-fouling property of membranes. J Memb Sci 659:120770. doi: https://doi.org/10.1016/j.memsci.2022.120770
30. Leal DA, Kuznetsova A, Silva GM, et al (2022) Layered materials as nanocontainers for active corrosion protection: A brief review. Appl Clay Sci 225:106537. doi: https://doi.org/10.1016/j.clay.2022.106537
31. Zárybnická L, Mácová P, Viani A (2022) Properties enhancement of magnesium phosphate cement by cross-linked polyvinyl alcohol. Ceram Int 48:1947–1955. doi: https://doi.org/10.1016/j.ceramint.2021.09.279
32. Dehghanpour SB, Parvizian F, Vatanpour V, He T (2022) Enhancing the flux and salt rejection of thin-film composite nanofiltration membranes prepared on plasma-treated polyethylene using PVA/TS-1 composite. React Funct Polym 177:105329. doi: https://doi.org/10.1016/j.reactfunctpolym.2022.105329
33. Ye Q, Xu J-M, Zhang Y-J, et al (2022) Metal-organic framework modified hydrophilic polyvinylidene fluoride porous membrane for efficient degerming selective oil/water emulsion separation. npj Clean Water 5:23. doi: 10.1038/s41545-022-00168-z
34. Thompson AK, Hackett C, Grady TL, et al (2020) Development and characterization of membranes with PVA containing silver particles: A study of the addition and stability. Polymers (Basel). doi: 10.3390/POLYM12091937

35. Wilken R, Holländer A, Behnisch J (1998) Nitric Oxide Radical Trapping Analysis on Vacuum-Ultraviolet Treated Polymers. Macromolecules 31:7613–7617. doi: 10.1021/ma9802071
36. Wilken R, Holländer A, Behnisch J (1998) Quantitative Comparison Between Vacuum-Ultraviolet Irradiation and Remote Hydrogen Plasma Treatment of Hydrocarbon Polymers. Plasmas Polym 3:165–175. doi: 10.1023/A:1021839228919
37. Holländer A, Wilken R, Behnisch J (1999) Subsurface chemistry in the plasma treatment of polymers. Surf Coatings Technol 116–119:788–791. doi: https://doi.org/10.1016/S0257-8972(99)00297-2
38. Fan X, Cai J, Yan C, et al (2020) Atmospheric gaseous hydrochloric and hydrobromic acid in urban Beijing, China: detection, source identification and potential atmospheric impacts. Atmos Chem Phys Discuss 1–24. doi: 10.5194/acp-2020-1235
39. Dölle C (2012) Light as a tool: Using vacuum-UV excimer radiation for activation of polymer surfaces. Galvanotechnik 103:2108–2119.
40. Rajakumaran R, Boddu V, Kumar M, et al (2019) Effect of ZnO morphology on GO-ZnO modified polyamide reverse osmosis membranes for desalination. Desalination 467:245–256. doi: 10.1016/j.desal.2019.06.018
41. Kanagaraj P, Liu C, Rana D (2021) Effect of the different layered structural modification on the performances of the thin-film composite forward osmosis flat sheet membranes – A review. React Funct Polym 167:104981. doi: https://doi.org/10.1016/j.reactfunctpolym.2021.104981
42. Wang Z, Li H, Tang F, et al (2018) A Facile Approach for the Preparation of Nano-size Zinc Oxide in Water/Glycerol with Extremely Concentrated Zinc Sources. Nanoscale Res Lett 13:202. doi: 10.1186/s11671-018-2616-0
43. Shalaby MS, Abdallah H, Wilken R, et al (2022) Effect graphene oxide nanostructure/tannic acid on mixed polymeric substrate-surface modified RO membranes. J Appl Polym Sci 139:e53195. doi: https://doi.org/10.1002/app.53195
44. Kamal N, Ahzi S, Kochkodan V (2020) Polysulfone/halloysite composite membranes with low fouling properties and enhanced compaction resistance. Appl Clay Sci. doi: 10.1016/j.clay.2020.105873
45. Jiang X, Chuah CY, Goh K, Wang R (2021) A facile direct spray-coating of Pebax® 1657: Towards large-scale thin-film composite membranes for efficient CO2/N2 separation. J Memb Sci 638:119708. doi: https://doi.org/10.1016/j.memsci.2021.119708
46. Gharehnazifam Z, Dolatabadi R, Baniassadi M, et al (2022) Multiphysics modeling and experiments on ultrasound-triggered drug delivery from silk fibroin hydrogel for Wilms tumor. Int J Pharm 621:121787. doi: https://doi.org/10.1016/j.ijpharm.2022.121787
47. Rémiás R, Kukovecz Á, Darányi M, et al (2009) Synthesis of Zinc Glycerolate Microstacks from a ZnO Nanorod Sacrificial Template. Eur J Inorg Chem 2009:3622–3627. doi: https://doi.org/10.1002/ejic.200900308
48. Rashidian G, Lazado CC, Mahboub HH, et al (2021) Chemically and Green Synthesized ZnO Nanoparticles Alter Key Immunological Molecules in Common Carp (Cyprinus carpio) Skin Mucus. Int J Mol Sci. doi: 10.3390/ijms22063270
49. Yee CM, Hassan HA, Hassan ZAA, Ismail R (2012) Zinc glycerolate: Potential active for topical application. J Oil Palm Res 24:1287–1295.
50. Rojas R, Kovacheva D, Petrov K (1999) Synthesis and Cation Distribution of the Spinel Cobaltites Cu x M y Co3-(x+ y) O4 (M= Ni, Zn) Obtained by Pyrolysis of Layered Hydroxide Nitrate Solid Solution. Chem Mater 11:3263–3267.
51. Hu Y, Lu K, Yan F, et al (2016) Enhancing the performance of aromatic polyamide reverse osmosis membrane by surface modification via covalent attachment of polyvinyl alcohol (PVA). J Memb Sci 501:209–219. doi: 10.1016/j.memsci.2015.12.003
52. Shao F, Dong L, Dong H, et al (2017) Graphene oxide modified polyamide reverse osmosis membranes with enhanced chlorine resistance. J Memb Sci 525:9–17. doi: 10.1016/j.memsci.2016.12.001
53. Shalaby MS, Abdallah H, Cenian A, et al (2020) Laser synthesized gold- nanoparticles, blend NF membrane for phosphate separation from wastewater. Sep Purif Technol. doi: 10.1016/j.seppur.2020.116994